DRAFT VERSION DECEMBER 30, 2010
Preprint typeset using LaTeX style emulateapj v. 11/10/09

FIRST INTERFEROMETRIC IMAGES OF THE 36 GHz METHANOL MASERS IN THE DR21 COMPLEX

VINCENT L. FISH[1], TALITHA C. MUEHLBRAD[1,2], PREETHI PRATAP[1,3], LORÁNT O. SJOUWERMAN[4], VLADIMIR STRELNITSKI[5], YLVA M. PIHLSTRÖM[6,7], & TYLER L. BOURKE[8]

Draft version December 30, 2010

ABSTRACT

Class I methanol masers are believed to be produced in the shock-excited environment around star-forming regions. Many authors have argued that the appearance of various subsets of class I masers may be indicative of specific evolutionary stages of star formation or excitation conditions. Until recently, however, no major interferometer was capable of imaging the important 36 GHz transition. We report on Expanded Very Large Array observations of the 36 GHz methanol masers and Submillimeter Array observations of the 229 GHz methanol masers in DR21(OH), DR21N, and DR21W. The distribution of 36 GHz masers in the outflow of DR21(OH) is similar to that of the other class I methanol transitions, with numerous multitransition spatial overlaps. At the site of the main continuum source in DR21(OH), class I masers at 36 and 229 GHz are found in virtual overlap with class II 6.7 GHz masers. To the south of the outflow, the 36 GHz masers are scattered over a large region but usually do not appear coincident with 44 GHz masers. In DR21W we detect an "S-curve" signature in Stokes V that implies a large value of the magnetic field strength if interpreted as due to Zeeman splitting, suggesting either that class I masers may exist at higher densities than previously believed or that the direct Zeeman interpretation of S-curve Stokes V profiles in class I masers may be incorrect. We find a diverse variety of different maser phenomena in these sources, suggestive of differing physical conditions among them.

Subject headings: ISM: molecules — magnetic fields — masers — radio lines: ISM — stars: formation

1. INTRODUCTION

Methanol masers are often found in star-forming regions. There are two sets of transitions seen to produce methanol masers. Class I methanol masers (most importantly the 36 and 44 GHz transitions) are believed to be collisionally excited, while class II masers (including the 6.7 and 12 GHz transitions) are radiatively excited (Cragg et al. 1992). Class I and class II methanol masers are sometimes both found in association with the same source (e.g., Slysh et al. 1994), but the two classes of masers are very rarely seen at the same velocity or in close (subarcsecond) spatial overlap.

Class I methanol masers, in which shocks dominate over infrared radiation, have often been assumed to be tracing an earlier evolutionary state of star formation than class II methanol, water, or OH masers (e.g., Ellingsen 2006; Breen et al. 2010). Subcategorization of class I masers by physical conditions may be possible (Sobolev 1993), leading some authors to speculate that line intensity ratios among the class I masers may be a proxy for evolutionary stage (Pratap et al. 2008). However, class I maser studies have traditionally been biased towards regions hosting other tracers of star formation, and the cluster environments in which class I masers are found are usually quite complex, calling into question traditional models of the evolutionary timeline of class I masers (Section 4.4 of Voronkov et al. 2010b, and references therein).

Furthermore, class I masers have typically been observed with single-dish telescopes, which can identify whether or not a particular class I transition produces masers in a region (and how bright they are) but do not have the resolution to determine their location relative to masers in other transitions. Given the complex environments associated with clustered star formation, high angular resolution is required to identify the relations between masers and excitation sources (e.g., Araya et al. 2009) and between multiple transitions of methanol (Voronkov et al. 2006). Higher angular resolution is also necessary to understand the physical conditions that produce masers in each of the class I transitions, which may not be identical (e.g., Menten 1991; Johnston et al. 1992; Sobolev 1993).

These concerns motivated Pratap et al. (2008) to do an unbiased single-dish search for class I methanol masers in nearby molecular clouds, resulting in the detection of new class I maser features. Several sites within these clouds host previously known 44 GHz methanol masers, many of which have been mapped interferometrically (e.g., Mehringer & Menten 1997; Kogan & Slysh 1998; Kurtz et al. 2004). Imaging the 36 GHz masers, the other bright transition seen in numerous sources (Haschick & Baan 1989; Berulis et al. 1990; Liechti & Wilson 1996; Pratap et al. 2008), has heretofore not been possible due to the lack of interferometers operating at this frequency. However, recent upgrades to the Australia Telescope Compact Array and the Expanded Very Large Array (EVLA) are allowing the first arcsecond-resolution images of 36 GHz masers to be produced (Sarma & Momjian 2009; Sjouwerman et al. 2010; Voronkov et al. 2010a). In this Letter, we report on the first EVLA maps of the 36 GHz masers in the DR21 star-forming

vfish@haystack.mit.edu
[1] MIT Haystack Observatory, Route 40, Westford, MA 01886, USA
[2] Current address: Texas Lutheran University, 1000 W. Court Street, Seguin, TX 78155, USA
[3] Current contact: ppratap2002@gmail.com
[4] National Radio Astronomy Observatory, P.O. Box O, Socorro, NM 87801, USA
[5] Maria Mitchell Observatory, 4 Vestal Street, Nantucket, MA 02554, USA
[6] Department of Physics and Astronomy, University of New Mexico, 800 Yale Boulevard NE, Albuquerque, NM 87131, USA
[7] Adjunct astronomer at NRAO
[8] Harvard-Smithsonian Center for Astrophysics, 60 Garden Street, Cambridge, MA 02138, USA

complex.

2. OBSERVATIONS AND DATA ANALYSIS

The EVLA was used to observe the 36.169 GHz $4_{-1} \rightarrow 3_0\ E$ line of methanol in DR21(OH), DR21W, and DR21N on 2010 May 26. The array consisted of the 20 telescopes outfitted with Ka-band receivers. The EVLA was in its most compact (D) configuration, providing a synthesized beamwidth of approximately $2\farcs1 \times 1\farcs4$. All three sources were observed in dual circular polarization centered on a fixed sky frequency of 36.1731 GHz and correlated with the new WIDAR correlator. The 4 MHz observing bandwidth was divided into 256 spectral channels, giving a velocity coverage of 33 km s^{-1} with a channel spacing of 0.13 km s^{-1}. Conversion from sky frequency to LSR velocity was performed with the assistance of the EVLA Online Dopset tool[9]. Total on-source observing time was ~ 12 min per source. Typical single-channel noise levels were $\lesssim 20$ mJy beam^{-1} near the center of the field

Data reduction was carried out using the NRAO Astronomical Image Processing System (AIPS). The flux scale was set using 3C48. Complex gain calibration was done using J2048+4310. EVLA transition issues precluded accurate bandpass calibration, although it could be determined from calibrator data that baseline phases were flat across the entire observing band and amplitudes were flat across about 75% of the observing band. Thus, our main results, including estimates of the positions of the detected masers, should not be significantly affected, although bandpass effects may lead to amplitude errors of a few percent over most of the observed velocity range. Data were imaged, and flux densities were corrected for primary beam attenuation.

Minor velocity errors may be introduced by two effects. First, the uncertainty in the rest frequency of the observed line ($36\,169.265 \pm 0.030$ MHz; Müller et al. 2004) is equivalent to a velocity uncertainty of 0.25 km s^{-1} (2 channels). Second, observations were performed at a fixed sky frequency, since Doppler tracking was unavailable. The sky frequency associated with the rest frequency drifted by about 0.015 MHz over the course of the observations, possibly resulting in an insignificant spectral broadening of maser features. Since the net uncertainty in determining the central velocity due to fixed-frequency observing ($<$ a few $\times 0.01$ km s^{-1}) is only a fraction of the channel separation (and much smaller than a typical maser linewidth), the data were not corrected with CVEL.

We present 229.758 GHz $8_{-1} \rightarrow 7_0\ E$ maser and 226 GHz continuum SMA data for all of our sources (P. Pratap et al., in preparation). The angular resolution of these observations is $\sim 1\farcs2 \times 0\farcs9$. The bandwidth of the 229 GHz observations covered the velocity range from −50 to +81 km s^{-1} with a spectral resolution of 0.13 km s^{-1}. The flux densities of the 229 GHz masers were corrected for primary beam attenuation. The rms noise near field center was approximately 0.15 Jy beam^{-1} for DR21(OH) and DR21N and 0.3 Jy beam^{-1} for DR21W.

When possible, we compare our data against three other class I methanol maser transitions from the literature: 44 GHz ($7_0 \rightarrow 6_1\ A^+$), 84 GHz ($5_{-1} \rightarrow 4_0\ E$), and 95 GHz ($8_0 \rightarrow 7_1\ A^+$). For DR21N, we also used archival 44 GHz data taken with the VLA in B-configuration on 2006 Jun 16.

[9] `http://www.vla.nrao.edu/astro/guides/dopset/`

3. RESULTS

Parameters of detected masers are listed in Table 1. We detect 49 36 GHz maser features in the three observed DR21 sources: 21 in DR21N, 23 in DR21(OH), and 5 in DR21W. Figures 1 and 2 show the locations of the 36 GHz masers relative to other class I methanol transitions mapped with interferometric resolution. The LSR velocities of detected masers are consistent with previous single-dish observations (Pratap et al. 2008).

Spectra of the integrated flux of individual 36 GHz maser features are often not well fit by a single Gaussian. In some cases multiple spectral peaks are evident, while in others there is evident skewness in the spectral peak. Both of these cases imply the existence of structure on scales smaller than our synthesized beam size (1–2″). Similar effects are seen in the 44 GHz transition, in which Kurtz et al. (2004) detect 17 masers in DR21(OH) (several with multiple spectral peaks) using 10 minutes of VLA D-configuration data, while Araya et al. (2009) detect 49 masers using a much longer integration of C-configuration data. When individual maser spectra in our data do show a single clear peak, we find that typical linewidths are on the order of 0.15 to 0.35 km s^{-1}. There is also a signature of very weak, extended methanol emission in some sources, but the lack of proper bandpass calibration tempers our confidence in this result.

There are 14 arcsecond-scale overlaps of a 36 GHz and a 229 GHz maser at approximately the same velocity ($|v_{36} - v_{229}| \lesssim 0.4$ km s^{-1}). Of these 14 associations, the 36 GHz maser is brighter in 7, and the 229 GHz maser is brighter in the other 7, indicating that either of the two $J_{-1} \rightarrow (J-1)_0\ E$ lines may be brighter (with the caveat that the 36 and 229 GHz observations did not occur simultaneously and that maser variability is possible). A similar phenomenon is seen in the $J_0 \rightarrow (J-1)_1\ A^+$ series, where Kalenskii et al. (1994) find that while the integrated 95 GHz flux is in general higher than that at 44 GHz, the integrated fluxes of sources whose spectra consist of *narrow-velocity* 44 and 95 GHz features (where the two transitions presumably produce single masers in close spatial association) are comparable in the two transitions. Further high-resolution data will be necessary to examine the relation between the flux densities of different maser transitions seen in close spatial association with each other.

3.1. *DR21(OH)*

The most striking feature of the masers in DR21(OH) is the central region of the source, where numerous masers in all mapped transitions occur in an approximately elliptical structure (Figure 1). Araya et al. (2009) identify more than 30 masers at 44 GHz associated with two shocks in a bipolar outflow. To within the positional uncertainty of our observations, all 14 of the 36 GHz masers in the outflow region are coincident with the Araya et al. (2009) 44 GHz masers. The 84 and 95 GHz masers are all located within the outflow region, although the lower angular resolution of the observations ($8\farcs3 \times 6\farcs2$, Batrla & Menten 1988, and $6\farcs5 \times 4\farcs4$, Plambeck & Menten 1990, respectively) precludes more detailed analysis of multitransition positional coincidences. Many of the 229 GHz masers align with 36 GHz masers on the western side of the outflow, but they appear to be more coincident with the 44 GHz masers of Araya et al. (2009), especially in the eastern part of the outflow.

All transitions exhibit a redshift on the western side of the outflow and a blueshift on the eastern side. There is also a

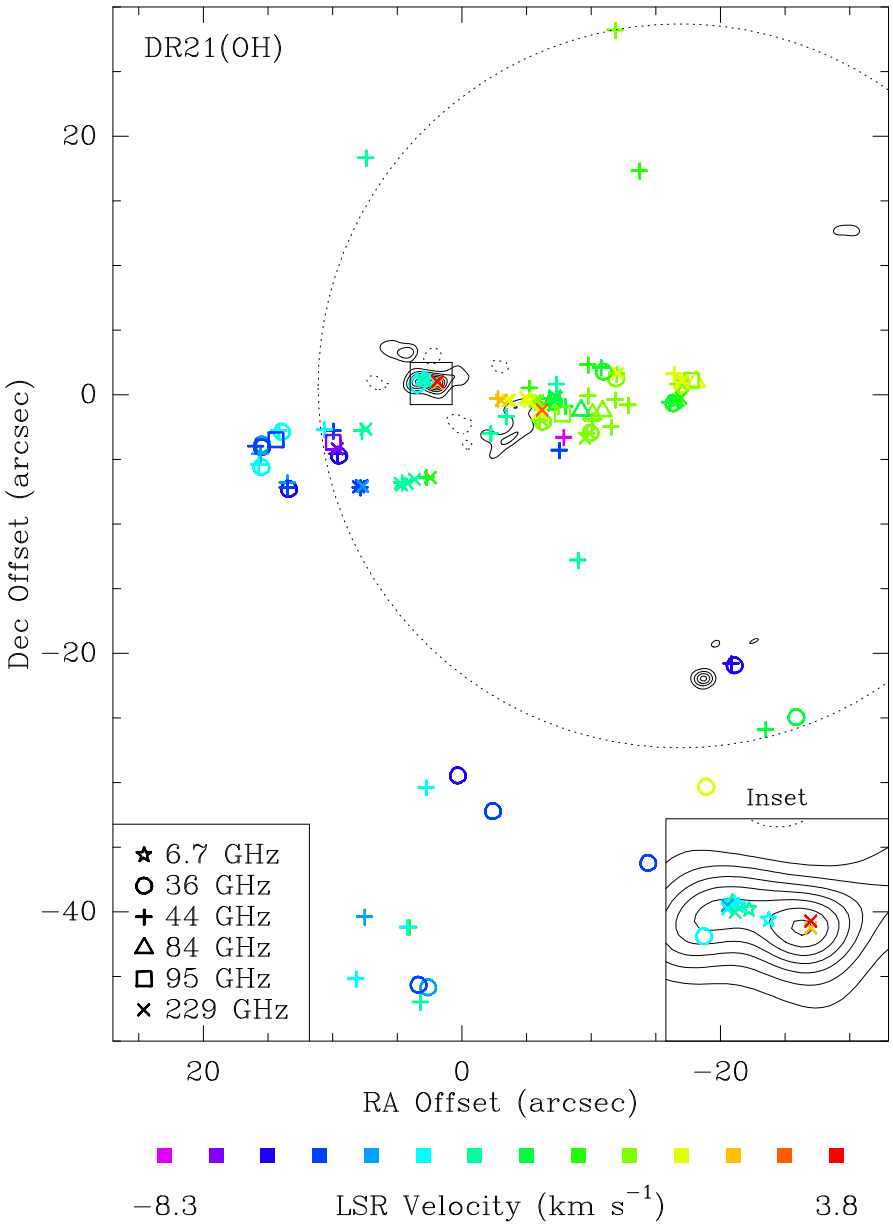

FIG. 1.— Class I methanol maser plot of DR21(OH) showing the 36 GHz (this work), 44 GHz (Araya et al. 2009), 84 GHz (Batrla & Menten 1988), 95 GHz (Plambeck & Menten 1990), and 229 GHz (P. Pratap et al., in preparation) class I transitions and the 6.7 GHz class II transition (Harvey-Smith et al. 2008). Contours indicate 226 GHz continuum (P. Pratap et al., in preparation). The angular resolution of the 84 and 95 GHz data was lower than for the 36 GHz masers and should therefore be taken as indicative only of the general distribution and velocity structure of the emission in these transitions, which are consistent with nearby class I masers in other transitions. The dotted circle indicates the primary beam of the 226 GHz continuum and 229 GHz maser observations. The inset box shows an enlargement of the 3.″25 square box near the origin, where 6.7, 36, and 229 GHz masers appear in close proximity and in the same velocity range. Coordinates are relative to the EVLA pointing center $20^{\rm h}39^{\rm m}00\overset{\rm s}{.}8, +42^\circ\,22'\,48\overset{''}{.}0$ (J2000).

general velocity gradient along the direction of the redshifted outflow to the west, with LSR velocities generally increasing from the center outward. Nevertheless, some of the masers on the northern and southern edges of the outflow have velocities that do not fit this pattern. The bright 36 GHz masers are located in the western side of the outflow, with the brightest 36 GHz maser being located very near the brightest 44 GHz (Araya et al. 2009) and 229 GHz masers.

Within the outflow, each detected 36 GHz maser is found in close spatial association with a 44 GHz maser at approximately the same velocity. The reverse is not true; that is, there are numerous 44 GHz features with no corresponding 36 GHz detection. On the eastern side of the outflow, 36 GHz masers are seen only at the eastern edge, while other transitions are seen throughout. In the central and western portions of the outflow, many of the 44 GHz masers, especially those that are highly redshifted or blueshifted compared to the velocity of the largest portion of the masers in the western outflow, have no accompanying 36 GHz features.

Class II masers in the 6.7 GHz transition ($5_1 \rightarrow 6_0\ A^+$) only appear projected atop the bright continuum feature near the origin in Figure 1 (Harvey-Smith et al. 2008). Several 229 GHz class I masers also appear, coincident with the 6.7 GHz masers in some cases at the 0.″1 level (one-tenth of

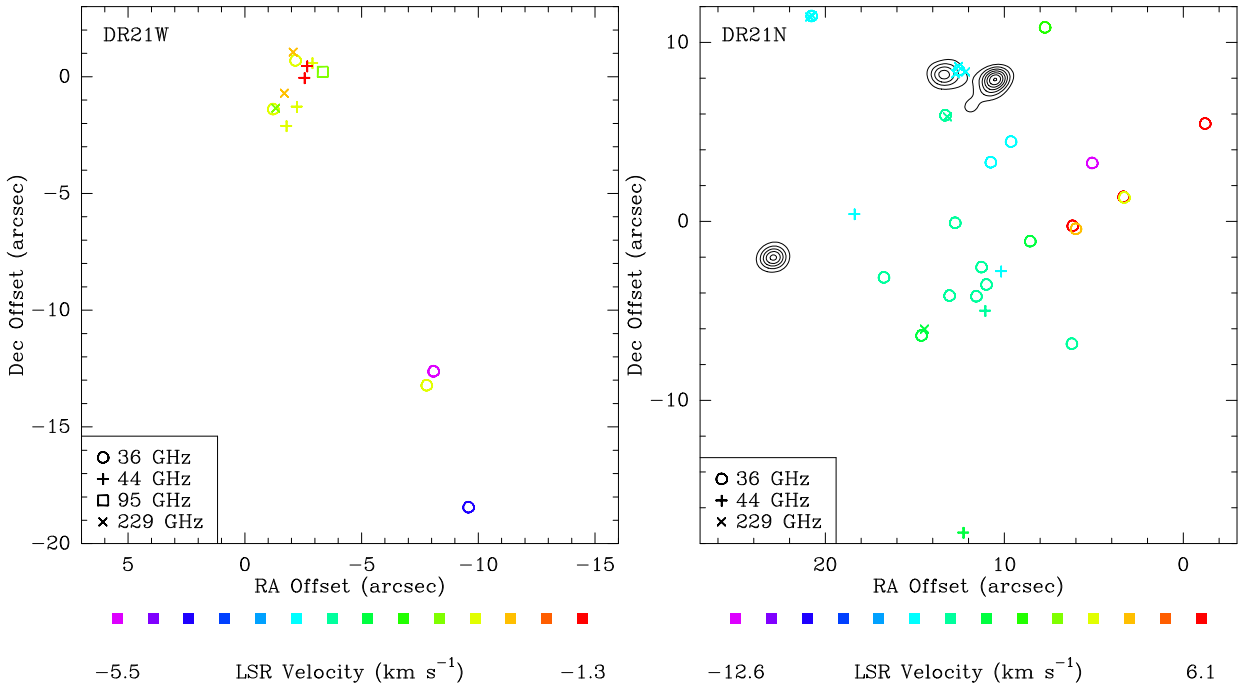

FIG. 2.— Class I methanol maser plots of DR21W (left) and DR21N (right). Symbols are as in Figure 1. The 44 GHz masers in DR21W are from Kogan & Slysh (1998). The 44 GHz data in DR21N were taken with the VLA in B-configuration. No 226 GHz continuum is detected in DR21W. Every 229 GHz maser in DR21N is found in close proximity to a 36 GHz maser. Coordinates are relative to the EVLA pointing center $20^h38^m55\overset{s}{.}0$, $+42°19'22\overset{''}{.}0$ for DR21W and $20^h39^m02\overset{s}{.}0$, $+42°25'43\overset{''}{.}0$ (J2000) for DR21N.

the 229 GHz beam size) but offset slightly to the east and south. We also detect weak 36 GHz maser emission in the region, with spots ranging from 100 to 150 mJy detected in eight spectral channels between –3.8 and –2.6 km s^{-1}, likely due to spectral blending of maser features that are not fully resolved at our resolution. We report the position of the strongest feature in Table 1. This feature is offset even farther to the east and south than the 229 GHz masers, with the caveat that it is difficult to determine the position of the 36 GHz maser accurately given the weakness of the maser and the 2″ beamsize of the 36 GHz observations.

Several class I masers appear to the south (36 and 44 GHz) and north (44 GHz only) of the outflow. Unlike in the outflow, the 36 GHz masers in the south are usually not accompanied by cospatial 44 GHz masers. The northern and southern masers are generally redshifted and blueshifted, respectively, compared to the bulk of the masers in the outflow, although not all masers conform to this pattern. The southern masers are located closer to the sources DR21(OH)W, DR21(OH)S, and the ridge of ammonia emission connecting them (Mangum et al. 1992; see also Sjouwerman et al. 2010) than to the outflow in DR21(OH), and therefore are unlikely to be associated with the main source driving the outflow in DR21(OH).

3.2. *DR21W*

Despite the detection of only 5 maser features, DR21W contains the brightest (> 80 Jy) 36 GHz maser in our sample. This maser is the only one for which we detect an antisymmetric Stokes V profile (Figure 3), which will be discussed further in Section 4.1. The bright masers near the origin in Figure 2 are coincident with the 44 GHz masers detected by Kogan & Slysh (1998) to better than a synthesized beamwidth. The velocities of the 36 GHz masers near the origin agree with the velocities of the brightest nearby 44 GHz masers to within 0.2 km s^{-1} or better.

3.3. *DR21N*

DR21N was first identified as a 36 GHz maser source by Pratap et al. (2008). We detect numerous 36 GHz masers in this source, mostly in the range from –6 to –4 km s^{-1}, on the eastern side of the distribution of maser emission (Figure 2). Several redshifted masers in the range –1 to +5 km s^{-1} are found on the western side, along with one highly blueshifted maser (–14 km s^{-1}). All detected 229 GHz masers are found in close proximity to (< 0.″5 from) a 36 GHz maser. In contrast, no 44 GHz maser is seen within 1″ of a 36 GHz maser.

4. DISCUSSION

4.1. *Circular Polarization*

As shown in Figure 3, we detect an antisymmetric "S-curve" Stokes V signature in the spectrum of the brightest maser in DR21W. If interpreted as due to Zeeman splitting, the implied line-of-sight magnetic field strength is $+58.1 \pm 6.2\,(1.7\,\mathrm{Hz\,mG^{-1}}/z)$ mG, where z represents the Zeeman splitting coefficient (assumed to be 1.7 Hz mG^{-1} for the 36 GHz transition by Sarma & Momjian 2009). The direction of this component of the magnetic field would be oriented away from the observer. The full three-dimensional field strength would presumably be larger, as Zeeman splitting measures only the line-of-sight component of the magnetic field when the splitting between Zeeman components is much less than the line width (Watson & Wyld 2001; Vlemmings 2008). Stokes V S-curves were not detected in any of the other maser sources, with a 3σ upper limit of $73\,(1.7\,\mathrm{Hz\,mG^{-1}}/z)$ mG in the brightest remaining maser in DR21(OH), although we note that a

TABLE 1
DETECTED MASERS

Source	RA Offset (arcsec)	Decl. Offset (arcsec)	v_{LSR} (km s^{-1})	Peak Flux Density (Jy)
DR21N	–1.21	5.46	6.07	0.96
	3.30	1.33	0.76	23.72
	3.35	1.36	5.42	0.17
	5.10	3.25	–12.58	0.31
	6.01	–0.43	3.22	0.40
	6.19	–0.26	6.07	0.19
	6.24	–6.84	–3.38	1.63
	7.73	10.83	–1.31	0.28
	8.56	–1.12	–2.61	0.28
	9.63	4.45	–4.94	0.25
	10.77	3.29	–5.71	0.18
	11.01	–3.54	–4.42	0.96
	11.28	–2.57	–4.42	0.37
	11.57	–4.19	–4.16	0.65
	12.54	8.44	–5.71	0.15
	12.75	–0.09	–4.42	0.31
	13.07	–4.16	–4.03	0.60
	13.30	5.92	–4.16	0.36
	14.64	–6.39	–3.12	10.08
	16.74	–3.14	–4.03	0.22
	20.77	11.47	–5.20	6.46
DR21(OH)	–25.86	–24.96	–1.48	2.66
	–21.08	–20.95	–6.01	0.36
	–18.88	–30.34	0.47	2.67
	–16.99	0.75	0.47	30.26
	–16.34	–0.68	–1.35	1.26
	–14.39	–36.24	–5.62	0.60
	–11.92	1.25	–0.05	1.31
	–10.96	1.77	–1.35	0.52
	–10.52	–1.72	–0.57	1.49
	–9.93	–2.98	0.08	10.39
	–7.10	–0.57	–1.61	2.39
	–6.24	–2.10	0.08	1.81
	–2.38	–32.23	–5.49	0.82
	0.33	–29.47	–5.88	0.54
	2.63	–45.86	–4.20	7.61
	3.38	–45.66	–5.62	0.86
	3.45[a]	0.78	–3.68	0.15
	9.52	–4.73	–6.53	1.69
	13.40	–7.31	–5.88	0.42
	13.94	–2.89	–3.55	0.50
	15.48	–3.87	–4.71	0.85
	15.49	–4.07	–4.97	0.54
	15.54	–5.61	–3.68	0.46
DR21W	–9.57	–18.45	–4.90	0.30
	–8.08	–12.63	–5.54	0.43
	–7.78	–13.23	–2.31	0.93
	–2.16	0.69	–2.44	24.60
	–1.21	–1.40	–2.44	82.29

NOTE. — Offsets are measured from $20^h39^m00\overset{s}{.}8$, $+42°22'48\overset{''}{.}0$ (J2000) for DR21(OH), $20^h39^m02\overset{s}{.}0$, $+42°25'43\overset{''}{.}0$ for DR21N, and $20^h38^m55\overset{s}{.}0$, $+42°19'22\overset{''}{.}0$ for DR21W.
[a] Brightest channel of spectrally-broad weak emission; see Section 3.1.

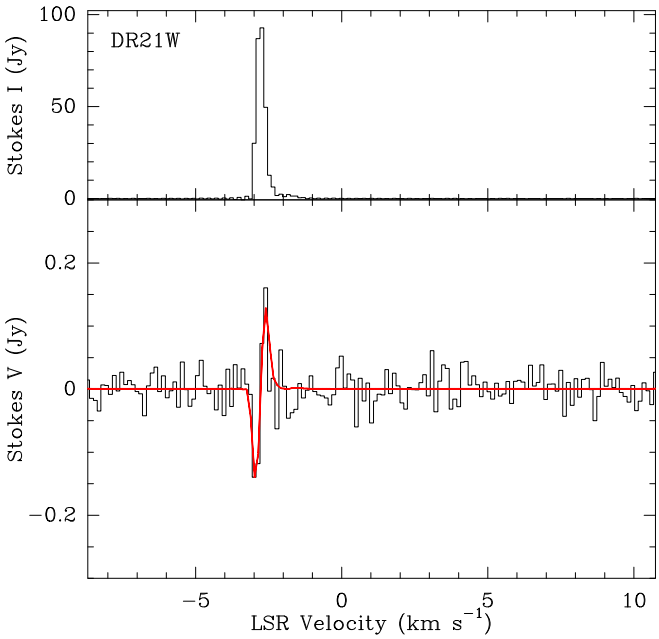

FIG. 3.— *Top*: Stokes I spectrum of a $\sim 6''$ rectangular region around the brightest maser feature in DR21W. *Bottom*: Stokes V spectrum after a scaled version of Stokes I has been subtracted. The thick red curve shows the best-fit value of the scaled derivative of Stokes I. The detection of an "S-curve" in Stokes V, discussed in Section 4.1, is significant even if the spectra are Hanning smoothed to reduce the ringing evident in Stokes I.

circular polarization fraction of $\sim 0.2\%$ (i.e., the V/I seen in DR21W) would not produce a detectable ($> 3\sigma$) Stokes V signal in DR21(OH) or in any of the weaker masers.

However, there is significant uncertainty in the Zeeman splitting coefficient, which calls into question the direct Zeeman interpretation of methanol Stokes V S-curves. Jen (1951) obtained a laboratory estimate of the Landé g-factor for the 25 GHz $J_2 \rightarrow J_1$ series of transitions of methanol, but the obtained value is an average over several different transitions and, in any case, may not be appropriate for the 36 GHz transition of methanol. Vlemmings et al. (2006) and Vlemmings (2008) used the Jen (1951) g-factor to estimate the Zeeman splitting coefficient for the 6.7 GHz transition, and Sarma & Momjian (2009) followed their method in deriving the Zeeman splitting coefficient at 36 GHz. A more recent look suggests that these calculations may have overestimated the Zeeman splitting coefficients by an order of magnitude (W. H. T. Vlemmings 2010, private communication), which would serve to *increase* proportionally the putative magnetic field strengths reported from methanol Zeeman splitting in this work and others (e.g., Vlemmings 2008; Surcis et al. 2009; Sarma & Momjian 2009, 2010).

Even if the Sarma & Momjian (2009) Zeeman splitting coefficient for the 36 GHz transition is (approximately) correct, a line-of-sight magnetic field strength of 58 mG is uncomfortably high. Measurements of the magnetic field strength are often used as a proxy for density. Using a scaling of $|B| \propto n^{0.47}$ from the densities and magnetic fields of DR21 would give a number density around 10^{10} cm^{-3} (Crutcher 1999), a value several orders of magnitude higher than that though to be suitable for 36 GHz maser excitation (e.g., Menten 1991; Johnston et al. 1992; Sobolev et al. 2005). Scaling from values typically found in OH masers instead (a few milligauss, $n \approx 10^6$ cm^{-3}; Pavlakis & Kylafis 1996; Fish et al. 2005) results in density estimates well in excess of 10^8 cm^{-3}, which is still substantially larger than theoretical estimates (but see also Section 4.3 of Voronkov et al. 2005). The discrepancy between the implied density and theoretical calculations appropriate for class I maser activity grows by two orders of magnitude if a smaller Zeeman splitting factor is assumed (W. H. T. Vlemmings 2010, private communication).

If the Zeeman interpretation is correct, one possible explanation for the discrepancy is that the correlation between magnetic field strength and density does not hold in (all) the environments of class I methanol masers, implying that the magnetic energy density is much greater than the kinetic energy

density (Sarma & Momjian 2009). Alternatively, it is possible that the high density implied by the large magnetic field is correct, and the bright 36 GHz maser in DR21W is produced via a pumping scheme not normally assumed for class I masers. Typically, class I masers are thought to be produced by collisional excitation followed by spontaneous cascade down to lower energy levels, with sink photons escaping or being absorbed by cold dust. This mechanism has an upper limit for density, above which the inverted transition is thermalized by collisions. One possible pumping mechanism at higher densities involves collisional excitation by a warm species and a collisional sink by a cooler species to produce the population inversion (Strelnitskij 1984). This mechanism requires a two-temperature mixture of particles, such as electrons (and/or ions) and neutrals, that may exist after the passage of a shock front. In principle, such a collisional-collisional pump can operate at arbitrarily high density, as long as the temperature difference between the two species is sustained.

However, it is more probable that the Stokes V signature we detect does not measure the magnetic field directly. Wiebe & Watson (1998) proposed a mechanism by which changes in the magnetic field orientation can convert linear polarization to circular polarization along the amplification path in a maser. The Stokes V signature produced by this mechanism can produce an S-curve that can mimic the effect of Zeeman splitting of a much larger magnetic field. In the case of circumstellar SiO masers that Wiebe & Watson (1998) consider, their proposed mechanism could operate with a magnetic field as weak as 0.1% of the magnetic field strength implied from interpreting the S-curve as purely due to Zeeman splitting. The Wiebe & Watson (1998) mechanism requires that the Zeeman splitting in units of frequency exceed both the stimulated emission rate and the decay rate appropriate for the masing transition, a condition likely to be satisfied for class I methanol masers (see Section 4.2 of Wiesemeyer et al. 2004).

Interestingly, DR21W (this work) and M8E (Sarma & Momjian 2009), the two sources with detected Zeeman splitting in the 36 GHz line, are also the two sources in which Wiesemeyer et al. (2004) detected circular polarization in the 133 GHz ($6_{-1} \rightarrow 5_0$ E) transition. Future high-sensitivity observations at 133 GHz might permit detection of an S-curve signature in Stokes V, thereby testing whether the magnetic field implied from a pure Zeeman interpretation is consistent with the values derived at 36 GHz. (Since the 36 GHz and 133 GHz methanol lines are both $J_{-1} \rightarrow (J-1)_0$ E transitions, the same Landé g-factor would be applicable to each of them.) Careful laboratory measurements of the Zeeman splitting coefficients appropriate for the brightest methanol maser transitions would also be very helpful.

4.2. *A Class I/Class II Overlap*

Excitation models indicate that the physical conditions that are thought to produce inversion in class I transitions usually lead to anti-inversion in class II transitions and vice versa (Cragg et al. 1992; Slysh et al. 2002). In that regard, the existence of class I 36 and 229 GHz masers at the same velocity and location as the class II 6.7 GHz maser site is surprising. These masers are also coincident with the brightest continuum emission near the outflow, which may be an important clue to their origin.

There is precedent for overlaps between class I and class II methanol masers. Voronkov et al. (2005) deduce spatial coincidences between the 6.7 GHz class II and 25 GHz $J_2 \rightarrow J_1$ E series of class I methanol masers in OMC-1, although the angular resolution of their interferometric observations is much poorer than either the 229 GHz data on which we report or the Harvey-Smith et al. (2008) 6.7 GHz data. Voronkov et al. (2005) model the 6.7/25 GHz overlap as arising from a lower-temperature regime than is typically assumed for class II masers. This pumping model requires an intermixed environment of gas and dust at a lower temperature ($\sim$ 60 K) than for traditional class II maser formation. The strong 226 GHz continuum emission in DR21(OH) likely marks such an environment that is rich in dust. The Voronkov et al. (2005) model did not investigate excitation at 229 GHz, but it does predict inversion at 36 GHz, which is also a $J_{-1} \rightarrow (J-1)_0$ E transition. The model predicts that 44 and 95 GHz masers should *not* appear at a low-temperature 6.7 GHz maser site, since the former are $J_0 \rightarrow (J-1)_1$ A^+ transitions, while the latter is a $(J-1)_1 \rightarrow J_0$ A^+ transition. Indeed, Kogan & Slysh (1998), Kurtz et al. (2004), and Araya et al. (2009) do not report 44 GHz masers at this location.

4.3. *Multitransition Comparison of Class I Masers*

In each of the sources we observed, the 36 GHz masers divide into two sets: those that are found to be cospatial with other class I maser transitions, and those that are spatially isolated. We address each of these two groups in turn.

In the outflow of DR21(OH) and in the cluster in the north of DR21W, we note that the distribution of the 36 GHz masers is similar to that of the 44, 84, 95, and 229 GHz masers. Additionally, the brightest masers in all of these transitions appear in the same location. In DR21(OH), the brightest masers in all class I transitions occur in a narrow velocity range ($v_{\rm LSR}$ = +0.3 to +0.5 km s^{-1}) at the western tip of the outflow. The next-brightest masers in each transition appear approximately 10″ east of this position (i.e., 10″ west of the origin in Figure 1). It is clear that these masers exist in a physical regime in which strong maser emission is produced in a large number of $J_{-1} \rightarrow (J-1)_0$ E and $J_0 \rightarrow (J-1)_1$ A^+ transitions simultaneously. The existence of a nearby energetic source creating an outflow likely shocks the surrounding molecular material, pumping multiple transitions of methanol in the same location.

On the other hand, all sources contain regions in which 36 GHz masers are not found to be coincident with other transitions. For instance, numerous masers in both the 36 and 44 GHz masers are found to the south of the outflow in DR21(OH). For the most part, the two transitions are not seen to be spatially coincident. Most of the 36 GHz masers and some of the 44 GHz masers in the south are seen near the periphery of CS emission (Plambeck & Menten 1990). The common feature of the environment of these masers is the lack of a nearby energetic source. As in the Sagittarius A region, it is possible that these masers trace molecular density clumps that are shock-excited by core collision or compression (Sjouwerman et al. 2010).

The 229 GHz masers appear to align more closely with the 44 GHz masers than with the 36 GHz masers in the DR21(OH) outflow. While 229 GHz masers are found to be coincident with 36 GHz masers on the western side of the outflow, there is always an accompanying 44 GHz maser. In contrast, several 229 GHz masers appear coincident with 44 GHz masers but without 36 GHz emission, especially on the eastern side of the outflow. However, we note several caveats about drawing conclusions from these points. First, the angu-

lar resolution of the observations of both the 44 GHz and the 229 GHz masers is higher than that of the 36 GHz observations on which we report, and it is possible that more sensitive, higher-resolution observations of the 36 GHz masers will uncover other features at the sites of the 44/229 GHz overlaps. Second, every detected 229 GHz maser in DR21N appears near a 36 GHz maser site (Figure 2). Third, at present the three DR21 sources on which we report are the only sources mapped in all three of the 36, 44, and 229 GHz transitions, and the field of view encompassed by the 229 GHz observations in DR21(OH) excludes nearly all of the masers south of the outflow as well as the eastern tip of the outflow itself. This constitutes a rather small set of sources from which to draw general conclusions about the properties of the 36, 44, and 229 GHz masers relative to each other. More interferometric observations of both the 36 and 229 GHz transitions will be required to fully understand the phenomenology of either.

5. CONCLUSIONS AND FUTURE WORK

We have interferometrically imaged three sources in the 36 and 229 GHz class I methanol maser lines. We find numerous masers in both transitions and a diversity of conditions among them. Notably, we identify the following three environments, each of which may correspond to a different set of excitation conditions.

1. The outflow in DR21(OH) contains a large number of overlaps in the 36, 44, and 229 GHz transitions. Strong emission is also seen at 84 and 95 GHz, although there is a lack of high-resolution observations of these lines. The brightest masers in all transitions appear at the same velocity and in the same location at the western tip of the outflow as traced by the masers.

2. The bright continuum source in DR21(OH) is associated with both the class II 6.7 GHz masers and class I 36 and 229 GHz E-type masers, but the class I 44 GHz A^+-type masers are conspicuously absent. This environment may be explained by the low-temperature intermixed dust and gas model of Voronkov et al. (2005).

3. The 229 GHz transition produces detectable masers at a subset of the 36 GHz maser sites in DR21N. In both this source and in DR21(OH) well south of the outflow, the 36 and 44 GHz masers have a similar large-scale distribution but are rarely found to produce a maser at the same site.

In addition, the brightest maser in DR21W produces an antisymmetric Stokes V profile that implies a large magnetic field if interpreted as being due to Zeeman splitting. There is a very large uncertainty in the Zeeman splitting coefficient appropriate for the 36 GHz transition, but the implied density (assuming $|B| \propto n^{\alpha}, \alpha \approx 0.5$) greatly exceeds the range over which class I masers are thought to form. It is possible that the circular polarization in this maser feature is produced by a much smaller magnetic field whose orientation changes over the amplification path of the maser (Wiebe & Watson 1998). In any case, careful laboratory measurement of Zeeman splitting coefficients appropriate for methanol maser transitions is warranted given the increasing number of Zeeman-like Stokes V signatures identified in methanol transitions over the past few years.

In order to realize the goal of being able to identify the physical conditions in a variety of star-forming regions by the presence or absence of various methanol maser transitions, it will be necessary to understand a few sources in greater detail. Our results highlight the need for both increased theoretical effort and more sensitive observations of multiple class I transitions at higher angular resolution. In particular, higher-resolution maps of the 84 and 95 GHz transitions as well as higher-frequency maser lines may be both enlightening and timely in the advent of the ALMA era. A further survey of sources in the 36 and 229 GHz transitions, when combined with 44 GHz maps in the literature, may also be helpful in determining the range of possible methanol excitation conditions in nature.

T. C. M. acknowledges support from the National Science Foundation's Research Experiences for Undergraduates program. The National Radio Astronomy Observatory is a facility of the National Science Foundation (NSF) operated under cooperative agreement by Associated Universities, Inc. The Submillimeter Array is a joint project between the Smithsonian Astrophysical Observatory and the Academia Sinica Institute of Astronomy and Astrophysics and is funded by the Smithsonian Institution and the Academia Sinica. We thank W. H. T. Vlemmings and A. Sarma for helpful discussions regarding methanol Zeeman splitting coefficients.

Facilities: EVLA (), SMA ()

REFERENCES

Araya, E. D., Kurtz, S., Hofner, P., & Linz, J. 2009, ApJ, 698, 1321
Batrla, W., & Menten, K. M. 1988, ApJ, 329, L117
Berulis, I. I., Kalenskii, S. V., & Logvinenko, S. V. 1990, Sov. Astron. Lett., 16, 179
Breen, S. L., Ellingsen, S. P., Caswell, J. L., & Lewis, B. E. 2010, MNRAS, 401, 2219
Cragg, D. M., Johns, K. P., Godfrey, P. D., & Brown, R. D. 1992, MNRAS, 259, 203
Crutcher, R. M. 1999, ApJ, 520, 706
Ellingsen, S. P. 2006, ApJ, 638, 241
Fish, V. L., Reid, M. J., Argon, A. L., & Zheng, X.-W. 2005, ApJS, 160, 220
Harvey-Smith, L., Soria-Ruiz, R., Duarte-Cabral, A., & Cohen, R. J. 2008, MNRAS, 384, 719
Haschick, A. D., & Baan, W. A. 1989, ApJ, 339, 949
Jen, C. K. 1951, Physical Review, 81, 197
Johnston, K. J., Gaume, R., Stolovy, S., Wilson, T. L., Walmsley, C. M., & Menten, K. M. 1992, ApJ, 385, 232
Kalenskii, S. V., Liljeström, T., Val'tts, I. E., Vasil'kov, V. I., Slysh, V. I., & Urpo, S. 1994, A&AS, 103, 129
Kogan, L., & Slysh, V. 1998, ApJ, 497, 800
Kurtz, S., Hofner, P., & Álvarez, C. V. 2004, ApJS, 155, 149
Liechti, S., & Wilson, T. L. 1996, A&A, 314, 615
Mangum, J. G., Wootten, A., & Mundy, L. G. 1992, ApJ, 388, 467
Mehringer, D. M., & Menten, K. M. 1997, ApJ, 474, 346
Menten, K. M. 1991, in ASP Conf. Ser. 16, Atoms, Ions and Molecules: New Results in Spectral Line Astrophysics, ed. A. D. Haschick & P. T. P. Ho (San Francisco: ASP), 119
Müller, H. S. P., Menten, K. M., & Mäder, H. 2004, A&A, 428, 1019
Pavlakis, K. G., & Kylafis, N. D. 1996, ApJ, 467, 309
Plambeck. R. L., & Menten, K. M. 1990, ApJ, 364, 555
Pratap, P., Shute, P. A., Keane, T. C., Battersby, C., & Sterling, S. 2008, ApJ, 135, 1718
Sarma, A. P., & Momjian, E. 2009, ApJ, 705, L176
Sarma, A. P., & Momjian, E. 2010, in International SKA Forum 2010 Science Meeting, PoS(ISKAF2010), 074
Sjouwerman, L. O., Pihlström, Y. M., & Fish, V. L. 2010, ApJ, 710, L111
Slysh, V. I., Kalenskiĭ, S. V., & Val'tts, I. E. 2002, Astronomy Reports, 46, 49
Slush, V. I., Kalenskii, S. V., Val'tts, I. E., & Otrupcek, R. 1994, MNRAS, 268, 464
Sobolev, A. M. 1993, Astron. Lett., 19, 293
Sobolev, A. M., Ostrovskii, A. B., Kirsanova, M. S., Shelemei, O. V., Voronkov, M. A., & Malyshev, A. V. 2005, in IAU Symp. 227, Massive Star Birth: A Crossroads of Astrophysics, ed. R. Cesaroni, M. Felli, E. Churchwell, & M. Walmsley (Cambridge: Cambridge Univ. Press), 174
Strelnitskij, V. S. 1984, MNRAS, 207, 339
Surcis, G., Vlemmings, W. H. T., Dodson, R., & van Langevelde, H. J. 2009, A&A, 506, 757
Vlemmings, W. H. T. 2008, A&A, 484, 773

Vlemmings, W. H. T., Harvey-Smith, L., & Cohen, R. J. 2006, MNRAS, 371, L26
Voronkov, M. A., Brooks, K. J., Sobolev, A. M., Ellingsen, S. P., Ostrovskii, A. B., & Caswell, J. L. 2006, MNRAS, 373, 411
Voronkov, M. A., Caswell, J. L., Britton, T. R., Green, J. A., Sobolev, A. M., & Ellingsen, S. P. 2010a, MNRAS, in press
Voronkov, M. A., Caswell, J. L., Ellingsen, S. P., & Sobolev, A. M. 2010b, MNRAS, 405, 2471
Voronkov, M. A., Sobolev, A. M., Ellingsen, S. P., & Ostrovskii, A. B. 2005, MNRAS, 362, 995
Watson, W. D., & Wyld, H. W. 2001, ApJ, 558, L55
Wiebe, D. S., & Watson, W. D. 1998, ApJ, 503, L71
Wiesemeyer, H., Thum, C., & Walmsley, C. M. 2004, A&A, 428, 479